Materials Today Communications 41 (2024) 110302

Contents lists available at ScienceDirect

Materials Today Communications

journal homepage: www.elsevier.com/locate/mtcomm

Efficient adsorptive removal of methyl green using Fe_3O_4/sawdust/MWCNT: Explaining sigmoidal behavior

Ismail Badran [a,*,1], Maan Omar Al-Ejli [b,2]

[a] Department of Chemistry, Faculty of Sciences, An-Najah National University, P.O. Box: 7, Nablus, Palestine
[b] Department of Chemistry and Earth Sciences, College of Arts and Sciences, Qatar University, P.O. Box: 2713, Doha, Qatar

ARTICLE INFO

Keywords:
Dyes water sustainability
Water pollutants
Methyl green
Iron oxide
Sawdust
Sigmoidal models

ABSTRACT

The 4R concept (reduce, reuse, recycle and repurpose) in water management necessitates innovative adsorption techniques that utilize sustainable and natural materials. This study investigates the use of natural sawdust embedded in magnetic iron oxide to treat wastewater. The performance of the newly synthesized Fe_3O_4/sawdust adsorbent was also compared to the native Fe_3O_4 and Fe_3O_4/MWCNT. Methyl Green (MG) was used as a model pollutant due to its wide use and potential toxicity. The new adsorbents demonstrated a high removal efficiency that exceeds 97 % under ambient conditions. The study investigates the effect of pH on adsorption, revealing a significant shift in removal efficiency as pH increases, with an optimal pH of around 7. The pH dependence is explained based on the point-of-zero-charge of the Fe_3O_4 adsorbent and the structure of the dye. The thermodynamic parameters (ΔH°, ΔS°, and ΔG°) of adsorption were determined through a temperature study. The adsorption equilibrium was found to be endothermic, therefore preferring elevated temperatures. Because the adsorption data of the study exhibited S-shaped-like curves, sigmoidal models were used to describe the adsorption isotherms. This provided new insights into the competitive adsorption mechanisms acting on the heterogeneous Fe_3O_4/sawdust surfaces. The kinetics study indicates rapid and efficient adsorption with pseudo-second-order reaction. The half-life of the reaction was as low as 4.8 min. The findings suggest a rapid, highly efficient and sustainable method to remove organic pollutants from wastewater.

1. Introduction

Our world is struggling with an alarming freshwater shortage marked by present wars, industrialization, misuse, droughts, natural disasters, and pollution. Estimates suggest that 2.2 billion people still lack access to safe drinking water worldwide [25,64,86]. Recent escalating conflicts have further intensified this crisis, creating further challenges for people seeking fresh water. Therefore, efforts are continued to develop efficient and accessible technologies that can secure freshwater for individuals and societies.

Over the course of recent decades, several technologies have been developed to address freshwater challenges such as flocculation, coagulation, adsorption, biodegradation, membrane removal, advanced oxidation, and ion exchange [6,7,23,73,77,81,82]. However, none of these methods are 100 % efficient, and therefore, a combination or a sequence of these techniques is usually adapted [1]. Also, the new technologies need to address new regulations, such as the zero liquid discharge (ZLD) and minimal liquid discharge (MLD) policies, that are put into place to limit pollutants discharged into the environment [11,24,60,65].

Adsorptive removal is the leading technique for cleaning water from both organic and inorganic contaminants [12,54,55,79,87,88]. Over the past few decades, extensive research has been done to prepare new types of nano-adsorbents that can quickly and efficiently clean water. These can be either engineered (e.g., free metals, metal oxides, and zeolites) or naturally occurring such as carbon nanotubes and clays [10,84,85]. [10] Because these materials are expensive and non-eco-friendly, there is a growing interest in green techniques that promote the use of affordable, natural alternatives like sawdust and food waste. This approach both serves the 4R concept (reduce, reuse, recycle and repurpose), as well as supports sustainable, and large-scale operations [5,34,36,67,72]. As such, the primary objective of this study is to explore the use of sawdust

* Corresponding author.
E-mail address: i.badran@najah.edu (I. Badran).
[1] ORCID ID: 0000-0003-1423-7124
[2] ORCID ID: 0000-0002-9713-4990

https://doi.org/10.1016/j.mtcomm.2024.110302
Received 22 February 2024; Received in revised form 17 June 2024; Accepted 1 September 2024
Available online 10 September 2024

waste as an adsorbent for water treatment, considering factors such as environmental sustainability, cost-effectiveness, and efficiency.

Organic industrial dyes are among the toughest pollutants to remove due to their complex aromatic structure [42,80]. Generally. organic dyes are categorized as mutagenic, allergenic, carcinogenic, toxic, and non-biodegradable [13,39,42]. Methyl green (MG) [$C_{26}H_{33}Cl_2N_3$, MG, Fig. 1] is an example of such dye, which is considered dangerous to humans and living organisms at high doses [1,8]. MG is a basic triphenylmethane-type di-cationic dye, featuring a complex aromatic structure that hinders its natural biodegradation. Its major applications include dyeing textiles, nylon, wool, silk, and cotton, along with its use as a pH indicator [7,8] Scheme 1.

While sawdust itself exhibits good adsorption properties [2,66], its separation from the aqueous medium hinders its applications. Hence, our objective was to synthesize a magnetic material incorporating sawdust to facilitate its separation and reuse. Iron oxides are examples of adsorbents that satisfy this requirement [20,30,46,57,63,68]. Magnetite (Fe_3O_4) is the most investigated mineral owing to its remarkable nanoscale qualities, such as its high stability, magnetism, and surface area [29,45,50,69]. However, pure Fe_3O_4 exhibits low adsorption efficiency. Throughout the reaction process, Fe_3O_4 tends to agglomerate, diminishing the specific surface area of the material by concealing the active sites on its surface. This ultimately results in a reduction of the catalytic activity of the catalyst [27,28].

Iron oxides can easily be functionalized to address specific contaminants [62]. This does not only emhamces the removal efficiency but can also bolsters their resistance to agglomeration. Surface modification can be carried out using solid supports like zeolite, sawdust, charcoal, carbon nanotubes, and activated carbon [2,11,12,15,75]. These materials have been recognized for their ability to serve as supports for magnetic nanoparticles and are acknowledged as excellent adsorbents frequently employed for organic pollutant adsorption in the environment.

Modeling of adsorption isotherms is crucial—not only for the sake of fitting the experimental data but also to interpret adsorption mechanisms and comprehend their nature [4,21,78]. Isotherms exhibit distinct types based on their curvature. While numerous adsorption data conform to conventional isotherms, such as Langmuir and Freundlich, other experimental data, including the present study, demonstrate a more complex nature, adhering to S-shaped isotherms (typified by Types II and IV), indicative of sigmoidal behavior. Consequently, an additional objective of this study is to identify the most suitable sigmoidal model that describes the adsorption behavior. The study also aims to provide an in-depth analysis of the causes of sigmoidal behavior.

Considering the motivations and objectives mentioned above, we investigated the effect of modifying the Fe_3O_4 surface with sawdust (SD), multi-walled carbon nanotubes (MWCNT), and activated carbon (AC). We studied the effects of adsorbent dosage, solution pH, shaking time, and temperature on MG adsorption, and correlated that with bare Fe_3O_4 The adsorption kinetics were investigated by monitoring the reaction over time till equilibrium is reached.

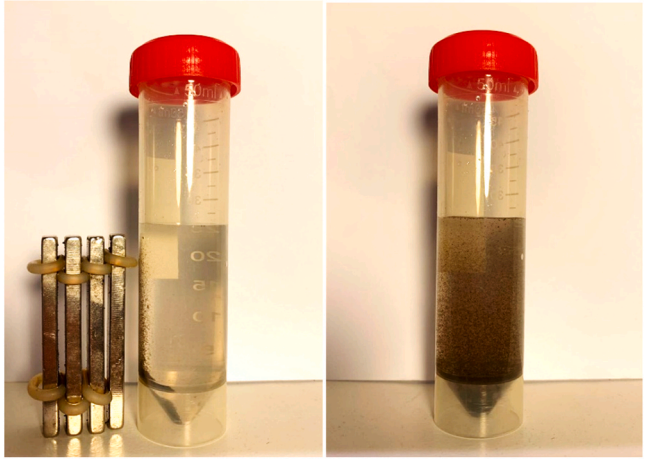

Fig. 1. Separating the Fe_3O_4 nanocomposite by a neodymium magnet.

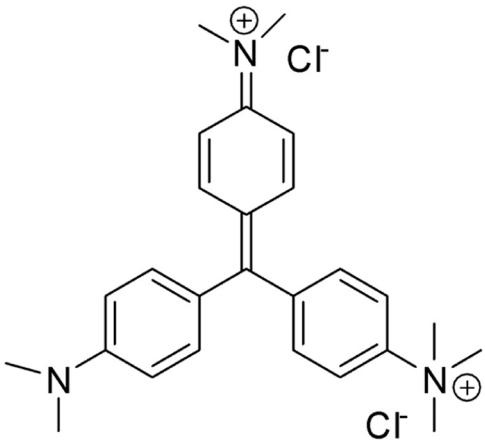

Scheme 1. Molecular structure of methyl green (MG).

2. Materials and methods

2.1. Materials and reagents

Methyl green ($C_{26}H_{33}Cl_2N_3$, 458.47 g/mol) was purchased from BDH Middle East LLC, Doha, Qatar. Iron (II) sulfate ($FeSO_4$, 99 %) and ammonium hydroxide (NH_4OH, 26 %) were obtained from Riedel-de Haen, Germany. Iron (III) sulfate hydrate ($Fe_2(SO_4)_3.xH_2O$, 400 g/mol, 99 %) was purchased from Research Lab Fine Chem, India. The sawdust (SD) used for this experiment was obtained from a local sawmill in Doha, Qatar. Multiwalled carbon nanotubes (MWCNT, outer diameter=5–15 nm, length= 10–30 μm) were acquired from Nanjing XFNano Material Tech Co. Ltd. China. Modified hydroxyethyl methyl cellulose (HEMC WALOCEL™ MKW 30000 PP30 Cellulose Ether) was obtained from Dow Chemical Company, Michigan, USA. Sodium hydroxide (NaOH, pellets, 97.5 %) and sodium nitrate ($NaNO_3$, 99 %) were purchased from Sigma-Aldrich Chemie GmbH, Taufkirchen, Germany, to be used in point-of-zero charge experiments. For preparing the buffer solutions, nitric acid (HNO_3, 69 %) and acetic acid (glacial, 99.55 %) were obtained from Loba Chemie Pvt. Ltd., India. Sodium acetate ($CH_3.COONa$, 99 %) was obtained from Research Lab Fine Chem., India. Ammonium chloride (99.5 %) was purchased from Sigma-Aldrich Chemie GmbH, Taufkirchen, Germany. The neodymium magnets (model DIYMAG, F60103, 20 P) used in this work were acquired from Amazon Inc., Washington, USA.

2.2. Instruments

For the adsorption studies, samples were weighed using a 5-digit analytical balance (Adam Equipment, UK). An ultrasonic cleaner (model 2800, Branson Ultrasonics Corporation, Connecticut, USA) was used to dissolve the samples once needed. The samples were shaken during the experiments using an orbital/linear shaker (model Sk-O180-PRO, Biobase Ltd., India). The shaking power and speed were sat at 15 W and 300 rpm, respectively. For the temperature study, a 28.0-L water bath equipped with a shaker (model NE5–28, Nickel-Electro Ltd. UK) was used. The pH was measured using a portable pH Meter (PH400S, Apera Instruments, Ohio, USA). The concentration changes of MG were followed by observing its maximum absorbance using a UV-Vis Spectrophotometer (model UV-2700i, Shimadzu. Maryland, USA). An X-ray diffractometer (MiniFlex 2, Applied Rigaku Technologies, Inc., Texas, USA), equipped with nickel-filtered CuKa radiation (λ =

0.1564 nm) and operating at 30 kV and 15 mA, was employed to investigate the crystal structure of the nanocomposites. The XRD scans were performed for 2 hours at a scanning rate of 1.8°/min in the 10–30° range. The field emission instrument (Nova Nano SEM 450), operating at 5 kV and equipped with an energy dispersive X-ray analyzer (EDX, Bruker), was used to obtain the scanning electron microscope (SEM) images for the nano-adsorbent.

2.3. Synthesis

Magnetite (Fe_3O_4) nanoparticles were prepared using the co-precipitation method as described previously [17,58,74]. Briefly, 12.006 g of $Fe_2(SO_4)_3.xH_2O$ and 2.2062 g of $FeSO_4$ (molar ratio of 2:1) were dissolved in 80 mL of Milli-Q® water. Care was taken to initiate the reaction quickly to prevent the rapid oxidation of iron (II) ions to brown Fe_2O_3. Afterwards, specific amounts of loading materials (SD or MWCNT) along with ~ 0.70 g of HEMC, as a binder, were added to the reaction. For simplicity, the Fe_3O_4 /SD and Fe_3O_4 /MWCNT will be donated herein as IO/SD and IO/CNT, respectively. In order to maintain the pH > 10, 50 mL of concentrated NH_4OH solution (26 %) was added dropwise to the mixtures over 5 min. The result was the formation of Fe_3O_4 due to the precipitation of $Fe_2(SO_4)_3.xH_2O$ and of $FeSO_4$ in basic medium. Further additions of NH_4OH were added as needed to maintain a basic medium. The reaction was kept under continuous stirring for 3 hours at 60°C. Afterwards, the reaction mixture was allowed to cool down to room temperature, and the nanoparticles were separated by a powerful neodymium magnet, rinsed multiple times in Milli-Q® water, and dried overnight at 80°C.

2.4. Point-of-Zero-Charge (PZC) measurements

To determine the adsorbent's point-of-zero-charge (PZC), ten solutions with identical ionic strength but different pH values ranging from 1.0 to 12.0 were prepared. An acetate buffer (CH_3COOH/CH_3COONa) was prepared to control the solution's pH. The pH was adjusted with 0.1 M dilutions of HNO_3 or NaOH. To maintain constant ionic strength, 40.0 mL of 0.1 M $NaNO_3$ was introduced to each flask. The initial pH was measured with a pH meter and recorded. Then, 20.0 mg of freshly produced Fe_3O_4 adsorbent was added to each flask, and the solutions were agitated for 20 hours at 350 rpm. Once equilibrium had been achieved, the pH was tested and declared final. The initial pH and final pH values were plotted, and the PZS was found to be the point of intersection [11,13,16,83].

2.5. Adsorption experiments

The batch adsorption tests were carried out by adding different masses of the freshly produced nano-adsorbents to 25.0 mL of 15 mg/L MG aqueous solutions in 50 mL vials. The vials were sealed and shaken for 20 minutes at 300 rpm and 25 °C. Using a neodymium magnet, the solid MG nano-adsorbent was removed from the solution, and the supernatant was transferred to a clean flask. To avoid any side-adsorptions by the filter papers, no filtering was performed. The MG concentrations were then determined by recording their absorbance spectra at λ_{max} = 635 nm, followed by converting the absorbance to concentration using a calibration curve. For the temperature study, a similar procedure was used, with the reaction vials and starting materials initially placed in a water bath at the desired temperature, followed by shaking the solutions for 20 min at the same temperature. UV-Vis spectra were then obtained using temperature-controlled cuvettes.

3. Results and discussion

3.1. Adsorbent's characterization

The distinguishing feature of Fe_3O_4 is its magnetic function, allowing it to be easier to handle with a magnet. Fig. 1 illustrates how easily the nanoparticles are separated by the neodymium magnet. The nanocomposites were also examined by field emission electron scanning microscope (SEM). The images are shown in Fig. 2 for the native Fe_3O_4 (a, b), and the composites: IO/CNT (c, d), and IO /SD)(e, f). The bare Fe_3O_4 shows a rough morphology with medium pores as illustrated by the 50,000-x magnification in Fig. 2(b). The material shows minimal signs of contamination as shown in the figure, a conclusion that is supported by the EDX analysis presented below. Fe_3O_4 underwent significant change when mixed with MWCNT as depicted in Fig. 2(c, d). The images show the traditional 'spongy' morphology of the carbon nanotube fibres that are bound to the Fe_3O_4 surface [11,14]. As for the IO /SD nanocomposite, Fig. 2(e, f) shows an irregular, sharper and smoother surface with shattered edges, in agreement with iron oxide/-wood morphology [76]. As measured by SEM, the particle size in all composites varied between ~20–100 nm in width and 100 nm to a few μm in length, in agreement with our recent work [11,14].

To shed more light on the elemental composition of their surfaces, the samples were examined by EDX analysis, as detailed in the Supplementary Information Section. The EDX of Fe_3O_4 (Fig S1) shows signals for Fe and O only. The mass percent of iron in Fe_3O_4 was determined to be 73.4 %, a result close to the theoretical value of 72.4 %. As for the IO/CNT sample (Fig S2), carbon was 41 % by mass, indicating a high loading of MWCNT as a result of the strong loading between iron oxide and the nanotubes. The carbon's mass percent in the Fe_3O_4/SD (Fig S3) varied between 20 % and 50 %, depending on the prepared ratio. Furthermore, the EDX analysis did not identify any unexpected elements, indicating the absence of contaminants in the samples. Further characterization of the Fe3O4 used in this work can also be found in previous works [8,11,17].

3.2. Adsorption experiments

In order to determine the MG concentration in the adsorbed samples, its absorbance in the visible region was recorded as discussed in the experimental section. Fig. 3-a shows the room-temperature spectra for the standard solutions of MG with a maximum absorbance at λ_{max} = 635 nm. The results were used to construct a calibration curve as shown in Fig. 3-b. The error bars in the figure represent the standard deviation between three replicates. The data followed a linear fitting with an R^2 value of 0.99983.

The adsorption experiments were performed by shaking the 15 mg L^{-1} MG solution in different amounts of Fe_3O_4 (ranging between 1 and 100 mg) and comparing the connotations of MG before and after the adsorption. In this work, the removal efficiency is defined as:

$$\text{Removal efficiency} = \frac{C_o - C_e}{C_o} \times 100\%$$

where C_o and C_e (mg L^{-1}) are the initial and equilibrium concentrations of the dye in solution. The removal efficiency for the native Fe_3O_4 was determined to be as high as 95 % at room temperature and neutral conditions, as illustrated in Fig. 4-a. This reflects the relatively high binding between the MG molecule and the nano surface. To better optimize and understand the adsorption mechanism, the effects of different environmental parameters, including pH and temperature were investigated as discussed below.

3.3. Effect of solution's pH

The effect of the solution's pH on the adsorption of MG by Fe_3O_4 was studied in the pH range of 1–7, and the results are shown in Fig. 4-a (The investigation was not extended to the basic region as MG turns colorless at pH > 8). Notably, the removal efficiency exhibits a significant shift with increasing pH. The removal efficiency increases from nearly zero at low pH to over 95 % removal as the pH reaches neutral conditions. To

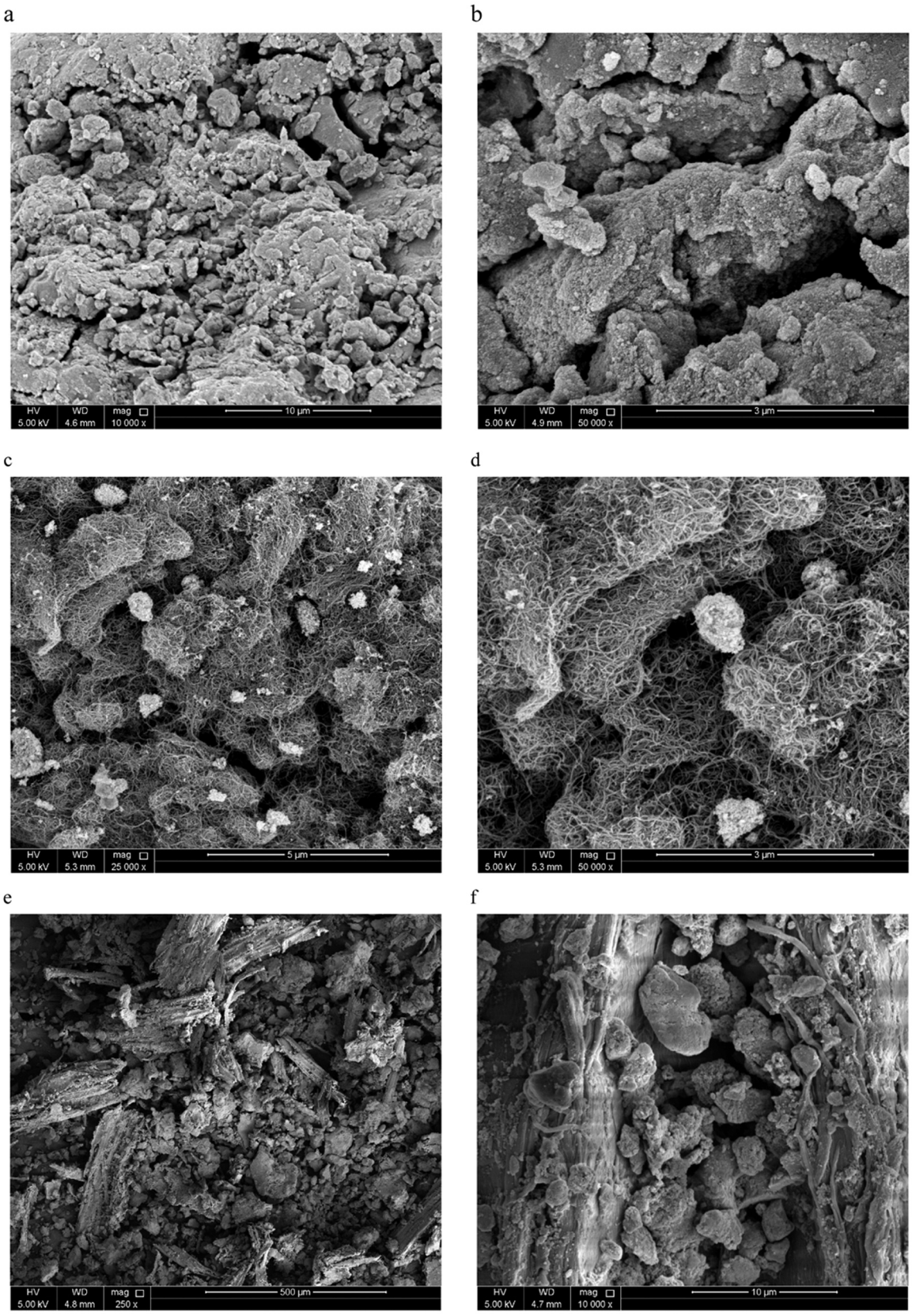

Fig. 2. Scanning electron microscope (SEM) images for a) native Fe_3O_4 (10,000x) b) native Fe_3O_4 (50,000x), c) Fe_3O_4/MWCNT (10,000x), d) Fe_3O_4/MWCNT (50,000x), e) Fe_3O_4/SD (10,000x),f) Fe_3O_4/SD (50,000x).

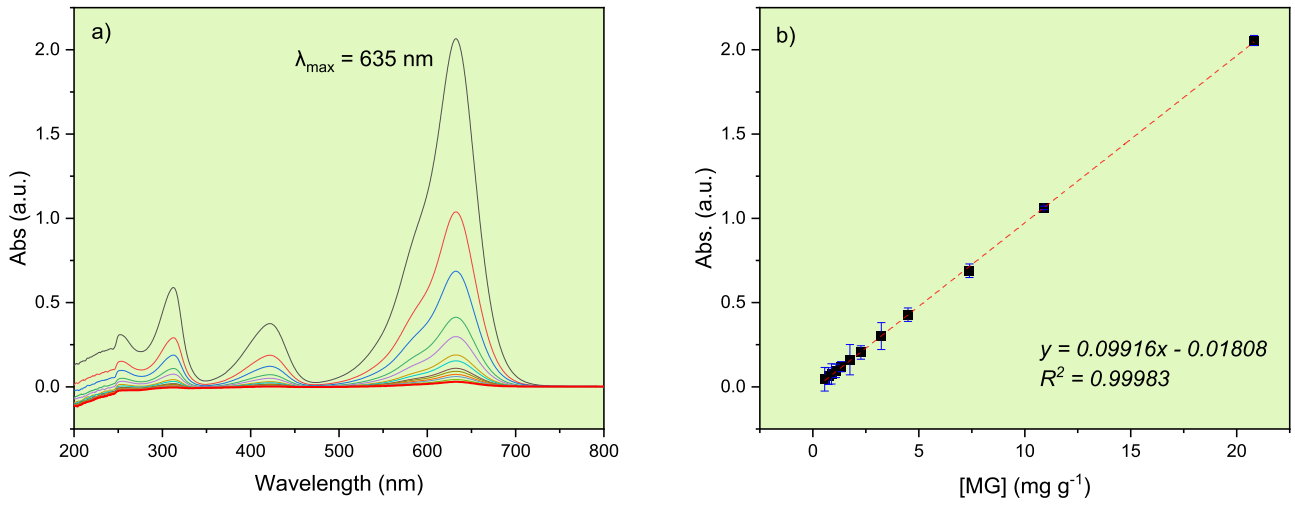

Fig. 3. a) room-temperature UV-Vis spectra for different concentrations of MG, b) linear fitting for the calibration curve for MG standard solutions at 25 °C, and pH ≈ 7. Error bars represent the standard deviations of three replicates.

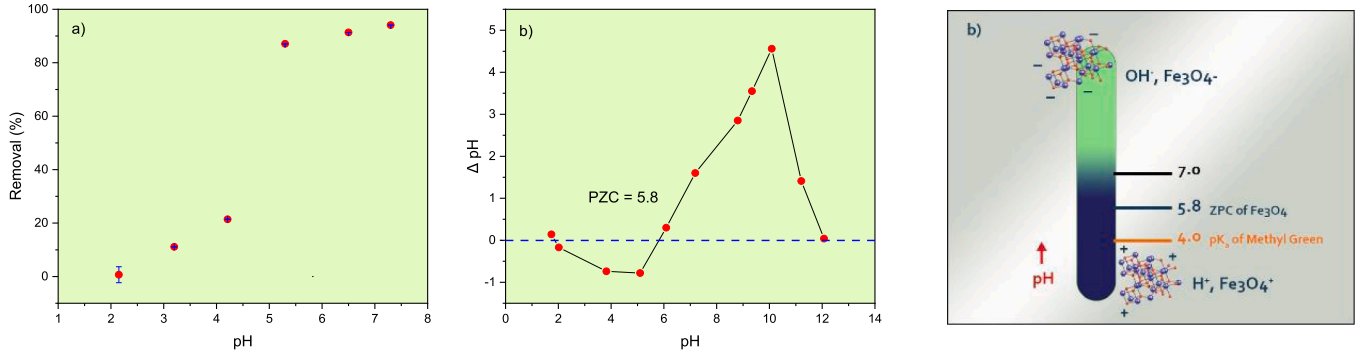

Fig. 4. Effect of solution's pH on the adsorption of 15 mg L^{-1} MG onto 80 mg of Fe_3O_4. Solution volume = 25 mL, T = 25°C. b) determining the point of zero charge for the Fe_3O_4 adsorbent, c) MG and Fe_3O_4 surface charges at different pH values.

better understand this behavior, the PZC of Fe_3O_4 was determined as described earlier. As shown in Fig. 4-b, the pH_{PZC} value is equal to 5.8. At a pH of 5.8, the Fe_3O_4 surface is electrically neutral; however, when the pH exceeds 5.8 or falls below 5.8, the surface possesses negative or positive charges, respectively. MG is a di-cationic dye with a reported pKa value of 4.0 [1]. However, previous reports indicate that the dye stays cationic within the pH range of 1–8 [7,44]. Thus, at low pH values, repulsive electrostatic interactions between the positively charged Fe_3O_4 surface and the cationic dye hinder its adsorption, leading to very low adsorption efficiency. As pH increases, the Fe_3O_4 surface becomes negatively charged as shown in Fig. 4-c. and strong interactions between the dye and the active sites dominate, leading to a high adsorption efficiency [37,43]. This finding is consistent with our recent work on Ketoprofen [11], and other studies that have used Fe_3O_4 as an adsorbent [61,70].

3.4. Effect of temperature

In this section, we discuss the effect of the solution's temperature on the adsorption of MG by Fe_3O_4. This serves to determine the thermodynamic parameters required to understand the adsorption mechanism. In a recent critical review by [48], it was observed that serious errors can occur in thermal analysis as a result of simplifying calculations. Several studies misapplied equations to determine thermal properties. The misuse involved employing a simplified Arrhenius plot without considering the equilibrium constant K, by plotting the natural logarithm of concentration against the reciprocal of temperature from a single experiment. This approach has led to substantial errors in assessing thermodynamic parameters. The authors emphasized the importance of "*obtaining isotherms of adsorption at different temperatures and making the nonlinear fitting of the isotherms*" to find the K values [11, 48]. Thus, we conducted our temperature investigation in accordance with these guidelines. The study was performed under isothermal conditions at five different temperatures: 282, 298, 315, 324, 338, and 347 K, The isothermal conditions were maintained by placing all solutions, materials, and glassware in a water bath at the desired temperature for at least 10 min. before the experiments to ensure thermal equilibrium. In addition, a temperature-controlled UV-Vis cuvette was used to minimize temperature fluctuations. The adsorption isotherms were constructed by plotting the adsorption capacity at equilibrium (q_e) vs. the adsorbate concentration at equilibrium (C_e), where the two are governed by the following relationship [11,13]:

$$q_e = \frac{C_0 - C_e}{W} V \quad (1)$$

In the above equation, C_o represents the initial concentration of MG in the solution (mg L^{-1}), V is the sample volume (L). and W is the mass of Fe_3O_4 nano adsorbents (g).

The thermodynamic parameters (ΔH°, ΔS°, and ΔG°) of adsorption can be deduced starting with the Van't Hoff equation [9,48]:

$$\Delta G^\circ = -RT\ln K_f \quad (2)$$

where ΔG° is the change in Gibb's free energy, R is the universal gas constant, and T is the temperature in K. The equilibrium constant K_f was

considered to be the Freundlich constant, defined in the formula:

$$q_e = K_F \quad C_e^{\frac{1}{n}} \tag{3}$$

where n is the Freundlich adsorption intensity. The fundamentals of thermodynamics state that:

$$\Delta G^{\circ} = \Delta H^{\circ} - T\Delta S^{\circ} \tag{4}$$

where ΔH° and ΔS° are the changes in standard enthalpy and entropy, respectively. Eqs. 2 and 4 rearrange to:

$$\ln K_f = \frac{-\Delta H^{\circ}}{RT} + \frac{\Delta S^{\circ}}{R} \tag{5}$$

Therefore, an Arrhenius plot of ln K_f vs. the reciprocal of T should give a straight line with a slope = -$\Delta H^{\circ}/R$ and an intercept = $\Delta S^{\circ}/R$.

The results of this investigation are illustrated in Fig. 5-a, with dashed lines representing non-linear fittings based on the Freundlich Eq. (3). All adsorptions have followed the Freundlich model with acceptable R^2 values that exceed 0.95, except the one at 282 K, which was disregarded. The fittings were used to determine the K_f values, which were then used to construct the Arrhenius plot in Fig. 5-b. The analysis of the slope and intercept of the plot as per Eq. 5 provided ΔH° and ΔG° values of 22.1 and −0.9 kJ mol^{-1}, respectively. The positive enthalpy change indicates that the adsorption of methyl green onto Fe_3O_4 is endothermic, in agreement with earlier observations involving $NiFe_2O_4$-CNT adsorbent. [15], Physically, a positive ΔH implies that, with increasing temperature, the adsorption equilibrium tends to shift to the right, promoting the formation of more adsorbate-adsorbent pairs. As a result, the removal efficiency increases to ~ 98 % at 347 K. On the other hand, the negative ΔG° value (-0.9 kJ mol^{-1}) indicates that the adsorption is slightly favored in the case of native Fe_3O_4. It was also determined that the entropy of adsorption (ΔS°) was 76.9 J mol^{-1} K^{-1}. This indicates that adsorbate-adsorbent pairs are more disordered than their individual counterparts.

3.5. Comparison between different modifications of Fe_3O_4 adsorbents

One aim of this work is to compare the adsorption efficiency of the cost-effective IO /SD adsorbent, with that of the native IO or IO/CNT composite. Fig. 6-a depicts the removal efficiency for the three adsorbents, with the concentration of MG, pH, shaking conditions, and temperature all kept constant. Clearly, the IO/CNT (red circles) has the highest adsorption efficiency in agreement with its superior ability to adsorb organic molecules [11,52,53]. To better assess the performance of the adsorbents, the adsorption isotherms are plotted in Fig. 6-b. The dashed lines represent non-linear fittings according to the corresponding-states equation (CSE) [41], which will be explained later. The maximum adsorption capacities, as obtained from the CSE model, were 2.7, 5.7, and 4.2 mg g^{-1} for IO, IO /10 %CNT and IO /10 %SD, respectively. It is noteworthy that the adsorption capacities of IO /10 % CNT and IO /10 %SD are remarkably close. In fact, our experiments demonstrated an impressive removal efficiency of 98 % with the use of 50 % sawdust-modified Fe_3O_4. This finding indicates that sawdust-modified iron oxide could be a great candidate for treating water from organic dyes, providing its low cost, availability, and toxicity.

3.6. Adsorption isotherms and interpretation of sigmoidal behavior

In this section, we discuss the modeling of adsorption isotherms of MG onto Fe_3O_4 modified with different loadings of 10 %, 25 %, and 50 % of sawdust. Generally, our data exhibited S-shaped curves as depicted in Fig. 7. The isotherms exhibited at least one inflection point, thereby categorizing them either as type II or IV according to the modern IUPAC classification [4,41].

We first fitted our data to the Langmuir [32,47], Freundlich [33], and Sips [32,71] models. The dashed lines in Fig. 7-a, b, and c, represent the results of these fittings. The fittings parameters and the R^2 values are tabulated in Table 1. The three traditional models proved inadequate in modeling the data, as evident in the figures and reflected by their R^2 being less than 0.95. An inflection point marks a location on a curve where the curvature undergoes a change. In other words, it signifies that the second derivative of the equation becomes zero. The inflection occurs due to the transition from low adsorbate concentration, where active sites are plenty, to high concentration, where the adsorption is limited by the number of active sites [41]. Therefore, we used modern models to describe the S-shaped behavior including the Langmuir-Sips [40,41], CSE [41], Sigmoidal Langmuir [49], Biphasic Sigmoidal [18], Biphasic Sigmoidal Dose-response [22,26], Meghea [56], and Anderson (modified BET) [21,35]. As seen in Table 1, the average R^2 values for sigmoidal models are all above 0.95. The best fittings were made by the Langmuir-Sips (R^2=0.960). CSE (R^2=0.986), Biphasic Sigmoidal Dose-response (R^2=0.995) and Anderson (R^2=0.974). The good performance of the CSE model to describe adsorption on modified iron oxide adsorbent is in agreement with our recent study on using Fe_3O_4/MWCNT to remove ketoprofen from aqueous solutions [11]. Although the Biphasic Sigmoidal Dose-response is widely used in toxicology and agriculture, it is seldom used in adsorption studies. Its great

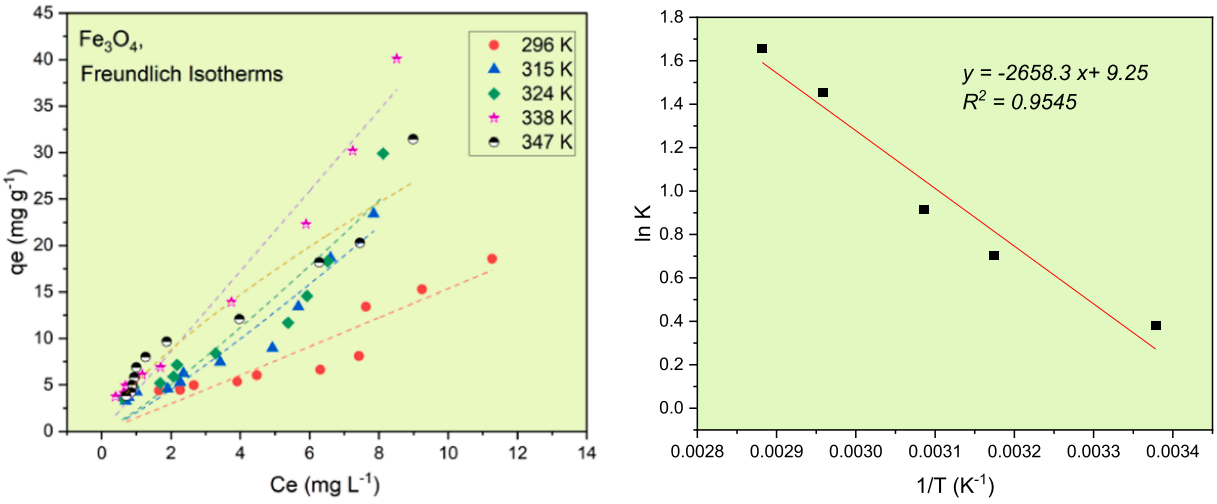

Fig. 5. a) Freundlich adsorption isotherms of MG at different temperatures, and b) Arrhenius plot of ln K vs. 1/T to determine the thermodynamic parameters for the adsorption of MG into the Fe_3O_4.

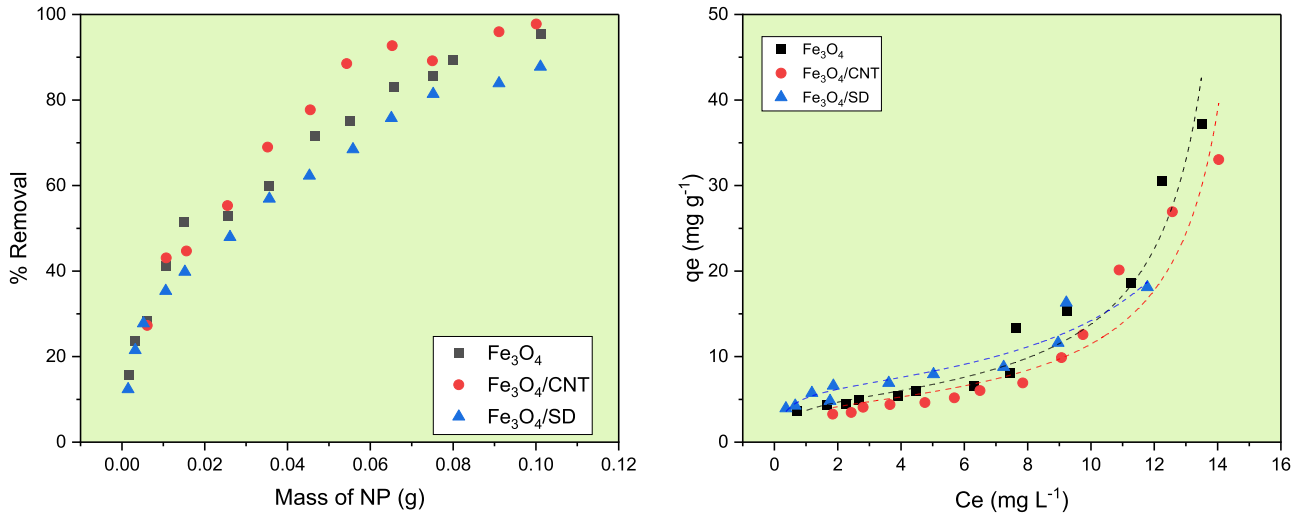

Fig. 6. a) Comparison of the removal efficiency of 15 mg L^{-1} MG by Fe_3O_4, Fe_3O_4/10 % sawdust, or Fe_3O_4/10 % MWCNT. b) adsorption isotherms according to the CSE model. Shaking time = 10 min, shaking speed = 300 rpm, T = 25 °C.

performance here (R^2 ≈1) is interesting. Its mathematical model (*cf.* Table 1-g) includes the A1 and A2 parameters, which respectively establish the maximum and minimum values for the 'dose'[18]. The A2 parameter becomes handy in this study in describing the maximum adsorption capacity (q_e), particularly when the curve converges to a horizontal plateau towards high concentrations, such as in the cases of IO and IO/10 %SD in Fig. 7-h. Similar observations can be made from the Biphasic Sigmoidal, Meghea, and Anderson curves (Fig. 7-g, I, and j).

It is significant to discuss the physical meaning of S-shaped isotherms. It is widely accepted that these isotherms may have two causes: either the adsorbate- adsorbate attractive forces at the surface may cause cooperative adsorption, or the adsorption is inhibited by a competing reaction. In fact, most studies agree that S-shaped behavior arises as a result of two opposite mechanisms [21,38,41,49]. In our case, the existence of two types of active sites, iron oxide and sawdust, leads to different adsorption mechanisms, in complete agreement with the ideas conveyed by Limousin [49].

3.7. Effect of contact time and adsorption kinetics

The adsorption kinetics of MG adsorption on IO/10 %SD was studied by following the concentration change over a period of 30 min. The concentration of MG, pH, shaking conditions, and temperature were all kept constant. Fig. 8 shows the results of this investigation along with non-linear fittings for pseudo first-order (PFO) and pseudo second-order (PSO) kinetics. The corresponding mathematical equations for the PFO and PSO models are [78]:

$$q_t = q_e \quad (1 - e^{-k_1 t}) \tag{6}$$

$$q_t = \frac{q_e^2 \quad k_2 t}{(1 + q_e k_2 \mathrm{t})} \tag{7}$$

where k_1 and k_2 are the pseudo first- and second-order rate constants, respectively.

The R^2 values for the PFO (0.9732) and PSO (0.9855) demonstrate that the adsorption in this study follows second-order kinetics. The estimated second-order rate constant is 2.32 × 10^{-4} mg^{-1} L s^{-1}. Therefore, the half-life of the reaction is 4.8 min. The half-life is in concert with previous studies on the adsorption of ketoprofen on IO/CNT (4.4 min)[11], and algae adsorption on porous carbon (8.4 min) [59]. It's worth noting that, according to the PSO model (41), the adsorbent material is characterized by an abundance of active sites, which contributes to the high efficiency of adsorption.

3.8. Comparison with previous studies

The above results suggest that the adsorption of MG using the modified iron oxides, IO/MWCNT and IO/SD, is rapid, efficient, and easy. In this section, we compare our findings with those from the literature. Table 2 shows a comparison between our results and those of prior research when MG was employed as an adsorbate and various engineered or natural adsorbents. First, there is an agreement on the optimal pH for the adsorption of MG, provided its structure and pKa as explained previously (section ↱3.3). The removal efficiency (>97 %) in this study is among the highest of all previous studies. Although Table 2 lists high efficiencies for adsorbents such as graphene oxide (GO), zeolites (e.g., MCM), and Silica gel/Polyaniline, our study holds an advantage due to the cost-effectiveness and availability compared to these engineered materials. In addition, the reaction kinetics of the IO/SD demonstrate quick adsorption with an equilibrium time of 30 min. This is also one of the fastest times as listed in Table 2. The most significant difference this study provides is the modeling of the adsorption isotherms. While previous studies on MG adsorption were confined to conventional models like Langmuir and Freundlich, this study employs sigmoidal models, offering new insights into the curvature, shape, and mechanism of adsorption.

4. Conclusions

In this study, we successfully demonstrated an efficient, rapid, and sustainable adsorptive removal of methyl green (MG), a widely used and toxic organic dye, from aqueous solutions. Adsorption was done using a newly synthesized sawdust-modified magnetite (Fe_3O_4/SD). The results were compared to the native Fe_3O_4 and Fe_3O_4/MWCNT, both prepared *in-situ*. The nanocomposites were characterized using SEM/EDX. While the native Fe_3O_4 exhibited a coarse morphology, the Fe_3O_4/CNT surface looked "spongy" as a result of the CNT fibers covering the iron oxide surface. The Fe_3O_4/SD, on the other hand, had irregular, sharper and smoother surfaces with shattered edges. The synthesized composites were found to be highly pure with rough surfaces. The nano adsorbents were highly magnetic and can be easily separated by a magnet. The adsorption was proved to be rapid, easy, and highly efficient. Both Fe_3O_4/SD and Fe_3O_4/CNT exhibited high removal efficiency exceeding 97 %. Adsorption was proved to be pH- dependent, with optimum adsorption occurring under near-neutral conditions. The pH effect was explained based on the point-of-zero-charge of Fe_3O_4 and the pKa of the dye. A temperature analysis, following recent literature

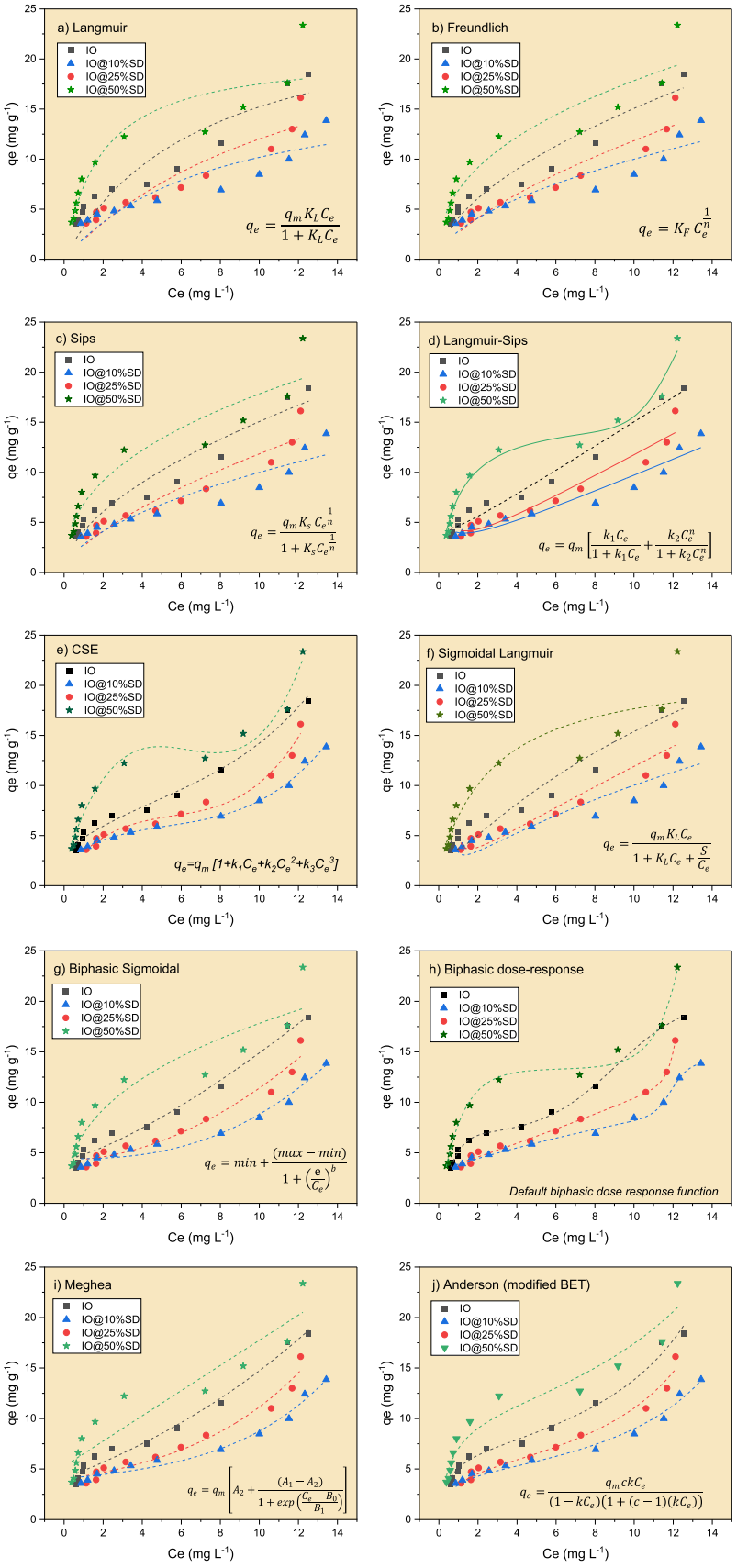

Fig. 7. Adsorption isotherms of MG onto IO/SD with non-linear fitting curves according to different models. Shaking time = 10 min, shaking speed = 300 rpm, T = 25 °C.

Table 1
Fitting parameters for the batch adsorption of MG according to different adsorption models.

Adsorption models fitting					
a) Langmuir					
$q_e = \frac{q_m K_L C_e}{1 + K_L C_e}$	Fe_3O_4	Fe_3O_4/10 %SD	Fe_3O_4/25 %SD	Fe3O4/50 %SD	Ave.
q_m	26.07	28.16	18.09	20.74	
K_L	0.140	0.074	0.129	0.539	
R^2	0.862	0.858	0.803	0.878	**0.850**
b) Freundlich					
$q_e = K_F C_e^{\frac{1}{n}}$					
K_f	4.107	2.795	2.619	6.856	
n	1.772	1.808	1.526	2.409	
R^2	0.936	0.875	0.902	0.907	**0.905**
c) Sips					
$q_e = \frac{q_m K_s C_e^{\frac{1}{n}}}{1 + K_s C_e^{\frac{1}{n}}}$					
q_m	6.88×10^{5}	2.72×10^{5}	3.20×10^{5}	9.54×10^{4}	
K_s	5.96×10^{-6}	1.03×10^{-5}	8.17×10^{-6}	7.19×10^{-5}	
n_S	0.565	0.554	0.656	0.415	
R^2	0.936	0.875	0.902	0.907	**0.905**
d) Langmuir-Sips					
$q_e = q_m\left[\frac{k_1 C_e}{1 + k_1 C_e} + \frac{k_2 C_e^n}{1 + k_2 C_e^n}\right]$					
q_m	2.21×10^{6}	5.11×10^{5}	4.85×10^{5}	1.59×10^{1}	
k_1	5.68×10^{-7}	1.65×10^{-6}	2.24×10^{-6}	8.98×10^{-1}	
k_2	1.54×10^{-6}	6.15×10^{-6}	6.57×10^{-6}	2.14×10^{-13}	
n	−0.133	−0.384	−0.568	11.617	
R^2	0.976	0.938	0.944	0.980	**0.960**
e) CSE					
$q_e = q_m[1 + k_1\, C_e + k_2\, C_e^2 + k_3\, C_e^3]$					
q_m	3.48	2.70	1.27	2.05	
k_1	0.41	0.46	1.92	2.97	
k_2	−0.033	−0.064	−0.298	−0.494	
k_3	2.30×10^{-3}	4.01×10^{-3}	1.77×10^{-2}	2.60×10^{-2}	
R^2	0.987	0.994	0.982	0.980	**0.986**
f) Sigmoidal Langmuir					
$q_e = \frac{q_m K_L C_e}{1 + K_L C_e + \frac{S}{C_e}}$					
q_m	46.8	37.8	161.2	22.2	
K_L	0.047	0.034	0.007	0.387	
S	−0.451	−0.654	−0.791	−0.147	
R^2	0.934	0.890	0.926	0.882	**0.908**
g) Biphasic Sigmoidal					
$q_e = \min + \frac{(\max - \min)}{1 + \left(\frac{e}{C_e}\right)^b}$					
Max	3.39×10^{5}	4.58×10^{5}	3.96×10^{5}	3.74×10^{5}	
Min	4.34	4.40	4.27	−1.28	
m	2.40×10^{4}	9.62×10^{2}	3.15×10^{3}	4.60×10^{12}	
b	1.33	2.53	1.90	0.37	
R^2	0.982	0.976	0.960	0.908	**0.956**
h) Biphasic dose-response					
$y = A1 + (A2 - A1)\left[\frac{p}{1 + 10^{(LOGx01 - x)h1}} + \frac{1 - p}{1 + 10^{(LOGx02 - x)h2}}\right]$					
A1	−4.6	−150.2	−20.7	−3690.7	
A2 (max)	20.5	20.7	518.8	5035.9	
h1	0.226	1.021	1.172	0.392	
h2	0.884	0.022	0.012	0.405	
p	0.552	0.027	0.446	0.576	
R^2	0.999	0.997	0.994	0.991	**0.995**
i) Meghea					
$q_e = q_m\left[A_2 + \frac{(A_1 - A_2)}{1 + \exp\left(\frac{C_e - B_0}{B_1}\right)}\right]$					
q_m	127.4	32.4	54.4	94.1	
Min (A_1)	−0.056	0.101	0.040	−10.56	
Max (A_2)	58.8	537.4	389.1	7.7	
B_0	96.9	51.9	58.3	−109.8	
B_1	14.88	5.20	6.22	334.24	
R^2	0.984	0.984	0.967	0.893	**0.957**
j) Anderson (modified BET)					

(*continued on next page*)

Table 1 (*continued*)

Adsorption models fitting					
$q_e = q_m\left[A_2 + \frac{(A_1 - A_2)}{1 + \exp\left(\frac{C_e - B_0}{B_1}\right)}\right]$					
q_m	6.82	4.61	5.22	10.44	
c	1.02	1.02	1.04	1.02	
k	−2.24	−2.27	−1.47	−1.70	
R^2	0.988	0.985	0.975	0.946	**0.974**

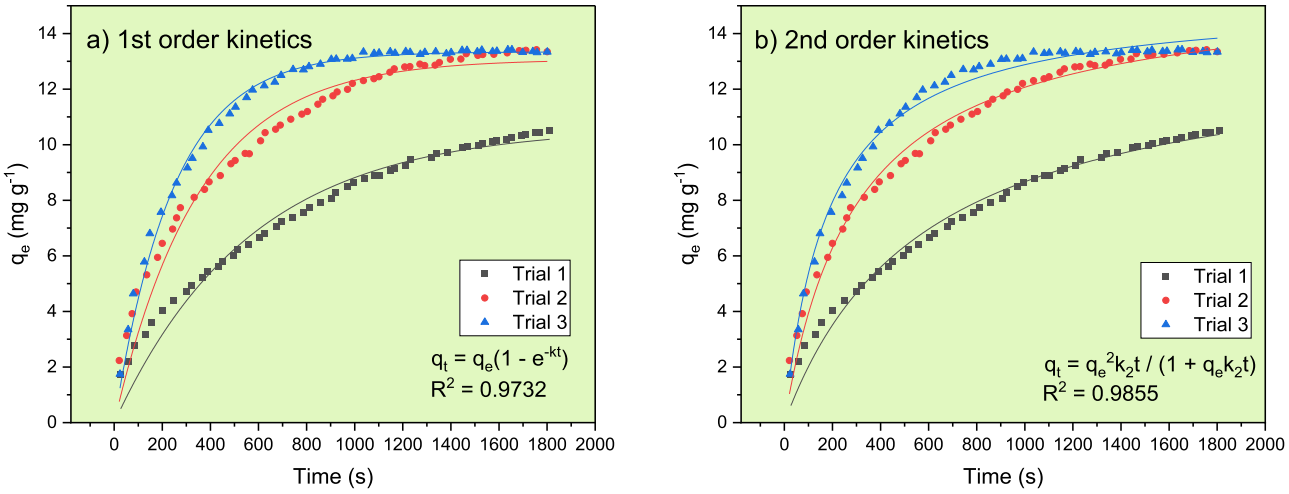

Fig. 8. The kinetics of adsorption of MG on IO/10 %SD modeled by a) nonlinear fitting for pseudo first-order, and b) second-order kinetics. MG concentration 15.0 mg L^{-1}, amount of adsorbent = 25 mg, shaking speed 350 rpm, shaking time = 10 min, solution pH ≈ 7. T = 25°C.

Table 2
Comparison between this study and other studies.

Adsorbent	Adsorbent particle size (nm)	Adsorption capacity (mg/g)	Concentration range (ppm)	Optimum pH	Equilibrium time (min)	Removal (%)	Isotherm model	Ref.
Eggshell waste	250000	70	1–100	6	105	69.38	Langmuir	Alalwan et al. [6]
Chitosan/Fe_2O_3/$NiFe_2O_4$	13.3	77.22	40	8	60	80	-	Ansari et al. [8]
MCM−41	5–100	285.70	10–50	6	60	99	Tamkin	Alardhi et al. [7]
$NiFe_2O_4$/CNTs	11	88.50	50–200	-	120	59	Langmuir	Bahgat et al. [15]
Silica gel/ Polyaniline	-	50	10–80	6	70	96	Freundlich	Belaib, Meniai [19]
GO/$CoFe_2O_4$	22.6	47.2	50–400	-	120	-	Langmuir	Farghali et al. [31]
$MgFe_2O_4$	10–25	1231	250–750	4	30	97.60	Langmuir	Liu et al. [50]
Halloysite nanotubes	100	185	10–300	6–7	120	95	Langmuir	M. Vargas-Rodríguez et al. [51]
Activated Sawdust-Based	100000	8.67×10^{-5} [a]	-	-	30	90	Langmuir	Rahman et al. [66]
Iron-manganese oxide/GO	10	195.7	20–100	8	160	94.60	Freundlich	Khan et al. [44]
TiO_2	5–10	384.6	50–200	6.3	45	-	Temkin and Langmuir	Abbas [1]
Bamboo	200000	5.5	5–30	-	140	79.40	Langmuir	Adnan Atshan [3]
Fe_3O_4	20–100	20.5[b]	1–16	7.0	30	95.5	Sigmoidal models	This work
Fe_3O_4/10 % MWCNT		35.5[b]				97.9		
Fe_3O_4/10 %SD		20.7[b]				97.8		

Author's Note: The observed maximum adsorption capacity appears surprisingly low.
[b] Based on the Biphasic dose-response model

recommendations, revealed that the adsorption is endothermic with ΔH°=22.1 kJ mol^{-1}, therefore favoring elevated temperatures. The ΔG° and ΔS° values were determined to be −0.9 kJ mol-1 and 76.9 J mol^{-1} K^{-1}, respectively. The adsorption isotherms for the Fe_3O_4/SD demonstrated an S-shaped curves. The traditional models of Langmuir, Freundlich, or Sips have failed to fit the data adequately. Thus, sigmoidal models were used to describe the isotherms. This includes the Langmuir-Sips, CSE, Sigmoidal Langmuir, Biphasic Sigmoidal, Biphasic Sigmoidal Dose-response, Meghea, and Anderson. It was found that the Biphasic Sigmoidal Dose-response was the best model with an R^2 close to unity (0.995). The fitting allowed the determination of the maximum adsorption capacity for the Fe_3O_4/SD to be 20.7 mg g^{-1}. The sigmoidal

behavior was explained based on the competing action theory. Because of the dual nature of the Fe_3O_4/SD adsorbent, and the availability of two different active sites, adsorption shifts between two different mechanisms passing through an inflection point on its isotherm's curve. The adsorption kinetics was also investigated by following the reaction over time. The reaction was found to follow pseudo-second order kinetics with a rate constant of 2.32×10^{-4} mg^{-1} L s^{-1}, and a half-life of 4.8 min, indicating rapid adsorption. Finally, the study's findings were compared with those in the literature, revealing the developed method's advantages. It boasts high adsorption efficiency and the benefit of utilizing natural sawdust waste for wastewater treatment.

CRediT authorship contribution statement

Ismail Badran: Writing – review & editing, Validation, Supervision, Resources, Project administration, Funding acquisition, Conceptualization. **Maan Omar Al-Ejli:** Writing – original draft, Investigation, Formal analysis, Data curation.

Declaration of Competing Interest

The authors declare that they have no known competing financial interests or personal relationships that could have appeared to influence the work reported in this paper.

Data Availability

Data will be made available on request.

Acknowledgements

The authors are grateful to the Department of Chemistry, and the Department of Chemistry at Qatar University for supporting this research. The author(s) would like to thank An-Najah National University (www.najah.edu) for the technical support provided to publish the present manuscript. The authors are also thankful to the staff at the Central Lab Unit (CLU) at Qatar University for helping in performing the SEM/EDX analysis.

Appendix A. Supporting information

Supplementary data associated with this article can be found in the online version at doi:10.1016/j.mtcomm.2024.110302.

References

[1] M. Abbas, Adsorption of methyl green (MG) in aqueous solution by titanium dioxide (TiO2): kinetics and thermodynamic study, Nanotechnol. Environ. Eng. *7* (3) (2022) 713–724, https://doi.org/10.1007/s41204-021-00178-1.
[2] K.A. Adegoke, O.O. Adesina, O.A. Okon-Akan, O.R. Adegoke, A.B. Olabintan, O. A. Ajala, O.S. Bello, Sawdust-biomass based materials for sequestration of organic and inorganic pollutants and potential for engineering applications, Curr. Res. Green. Sustain. Chem. *5* (2022) 100274, https://doi.org/10.1016/j.crgsc.2022.100274.
[3] A. Adnan Atshan, Adsorption of methyl green dye onto bamboo in batch and continuous system, Iraqi J. Chem. Pet. Eng. *15* (1) (2014) 65–72, https://doi.org/10.31699/IJCPE.2014.1.8.
[4] M.A. Al-Ghouti, D.A. Da'ana, Guidelines for the use and interpretation of adsorption isotherm models: a review, J. Hazard. Mater. *393* (2020) 122383, https://doi.org/10.1016/j.jhazmat.2020.122383.
[5] M. Al-Jabari, M. Abualfailat, S. Shaheen, Treating leather tanning wastewater with stone cutting solid waste, Clean. – Soil Air Water *40* (2) (2012) 206–210.
[6] H.A. Alalwan, M.M. Mohammed, A.J. Sultan, M.N. Abbas, T.A. Ibrahim, H.A. S. Aljaafari, A.A. Alminshid, Adsorption of methyl green stain from aqueous solutions using non-conventional adsorbent media: isothermal kinetic and thermodynamic studies, Bioresour. Technol. Rep. *14* (2021) 100680, https://doi.org/10.1016/j.biteb.2021.100680.
[7] S.M. Alardhi, J.M. Alrubaye, T.M. Albayati, Adsorption of methyl green dye onto MCM-41: equilibrium, kinetics and thermodynamic studies, Desalin. Water Treat. *179* (2020) 323–331.
[8] M.J. Ansari, S.A. Jasim, D.O. Bokov, L. Thangavelu, G. Yasin, A.D. Khalaji, Preparation of new bio-based chitosan/Fe2O3/NiFe2O4 as an efficient removal of methyl green from aqueous solution, Int. J. Biol. Macromol. *198* (2022) 128–134, https://doi.org/10.1016/j.ijbiomac.2021.12.082.
[9] P.W. Atkins, J. De Paula, J. Keeler. Atkins' Physical Chemistry, 11th Ed., Oxford University Press, London, UK, 2023.
[10] I. Badran, 9 - Natural, biosynthesized, polymeric, and other remediation nanoreagents, in: C.M. Hussain, N.N. Nassar (Eds.), Nanoremediation, Elsevier, 2023, pp. 259–281.
[11] I. Badran, M.O. Al-Ejli, Efficient multi-walled carbon nanotubes/iron oxide nanocomposite for the removal of the drug ketoprofen for wastewater treatment applications, ChemistrySelect *7* (38) (2022) e202202976, https://doi.org/10.1002/slct.202202976.
[12] I. Badran, M.O. Al-Ejli, N.N. Nassar, 2 - Applications of nanomaterials for adsorptive removal of various pollutants from water bodies, in: C.M. Hussain, N. N. Nassar (Eds.), Nanoremediation, Elsevier, 2023, pp. 25–62.
[13] I. Badran, R. Khalaf, Adsorptive removal of alizarin dye from wastewater using maghemite nanoadsorbents, Sep. Sci. Technol. *55* (14) (2020) 2433–2448, https://doi.org/10.1080/01496395.2019.1634731.
[14] I. Badran, O. Qut, A.D. Manasrah, M. Abualhasan, Continuous adsorptive removal of glimepiride using multi-walled carbon nanotubes in fixed-bed column, Environ. Sci. Pollut. Res. *28* (12) (2021) 14694–14706, https://doi.org/10.1007/s11356-020-11679-y.
[15] M. Bahgat, A.A. Farghali, W. El Rouby, M. Khedr, M.Y. Mohassab-Ahmed, Adsorption of methyl green dye onto multi-walled carbon nanotubes decorated with Ni nanoferrite, Appl. Nanosci. *3* (3) (2013) 251–261, https://doi.org/10.1007/s13204-012-0127-3.
[16] E.N. Bakatula, D. Richard, C.M. Neculita, G.J. Zagury, Determination of point of zero charge of natural organic materials, Environ. Sci. Pollut. Res. *25* (2018) 7823–7833.
[17] M. Baziar, A. Azari, M. Karimaei, V.K. Gupta, S. Agarwal, K. Sharafi, S. Dobaradaran, MWCNT-Fe3O4 as a superior adsorbent for microcystins LR removal: Investigation on the magnetic adsorption separation, artificial neural network modeling, and genetic algorithm optimization, J. Mol. Liq. *241* (2017) 102–113, https://doi.org/10.1016/j.molliq.2017.06.014.
[18] W.N. Beckon, C. Parkins, A. Maximovich, A.V. Beckon, A general approach to modeling biphasic relationships, Environ. Sci. Technol. *42* (4) (2008) 1308–1314, https://doi.org/10.1021/es071148m.
[19] F. Belaib, A.-H. Meniai, The removal of cationic dye (Methyl green) dye by adsorbant based Silica gel/Polymer, Algerian J. Eng. Res. *0* (2017) 39–43.
[20] R. Bhateria, R. Singh, A review on nanotechnological application of magnetic iron oxides for heavy metal removal, J. Water Process Eng. *31* (2019) 100845.
[21] C. Buttersack, Modeling of type II high-resolution sorption isotherms: evaluation of different approaches, Colloids Surf. A: Physicochem. Eng. Asp. *650* (2022) 129489, https://doi.org/10.1016/j.colsurfa.2022.129489.
[22] E.J. Calabrese, Biphasic dose responses in biology, toxicology and medicine: accounting for their generalizability and quantitative features, Environ. Pollut. *182* (2013) 452–460, https://doi.org/10.1016/j.envpol.2013.07.046.
[23] W.S. Chai, J.Y. Cheun, P.S. Kumar, M. Mubashir, Z. Majeed, F. Banat, P.L. Show, A review on conventional and novel materials towards heavy metal adsorption in wastewater treatment application, J. Clean. Prod. *296* (2021) 126589.
[24] B. Chuan Yee Lee, E. Tan, Y. Lu, H. Komori, S. Pietsch, R. Goodlett, M. James, Antiscalant and its deactivation in zero/minimized liquid discharge (ZLD/MLD) application in the mining sector – opportunities, challenges and prospective, Miner. Eng. *201* (2023) 108238, https://doi.org/10.1016/j.mineng.2023.108238.
[25] R. Connor, The United Nations world water development report 2015: water for a sustainable world, Vol. 1, UNESCO publishing, 2015.
[26] Corporation, O. (2021). OriginPro. In: OriginLab Northampton, MA, USA.
[27] X. Cui, S.-S. Zhang, Y. Geng, J. Zhen, J. Zhan, C. Cao, S.-Q. Ni, Synergistic catalysis by Fe3O4-biochar/peroxymonosulfate system for the removal of bisphenol a, Sep. Purif. Technol. *276* (2021) 119351, https://doi.org/10.1016/j.seppur.2021.119351.
[28] C.-D. Dong, C.-W. Chen, C.-M. Hung, Synthesis of magnetic biochar from bamboo biomass to activate persulfate for the removal of polycyclic aromatic hydrocarbons in marine sediments, Bioresour. Technol. *245* (2017) 188–195, https://doi.org/10.1016/j.biortech.2017.08.204.
[29] G. Fadillah, S.P. Yudha, S. Sagadevan, I. Fatimah, O. Muraza, Magnetic iron oxide/clay nanocomposites for adsorption and catalytic oxidation in water treatment applications, Open Chem. *18* (1) (2020) 1148–1166, https://doi.org/10.1515/chem-2020-0159.
[30] M. Faraji, N. Arianpouya, NiCoFe-layered double hydroxides/MXene/N-doped carbon nanotube composite as a high performance bifunctional catalyst for oxygen electrocatalytic reactions in metal-air batteries, J. Electroanal. Chem. *901* (2021) 115797, https://doi.org/10.1016/j.jelechem.2021.115797.
[31] A.A. Farghali, M. Bahgat, W.M.A. El Rouby, M.H. Khedr, Preparation, decoration and characterization of graphene sheets for methyl green adsorption, J. Alloy. Compd. *555* (2013) 193–200, https://doi.org/10.1016/j.jallcom.2012.11.190.
[32] K.Y. Foo, B.H. Hameed, Insights into the modeling of adsorption isotherm systems, Chem. Eng. J. *156* (1) (2010) 2–10, https://doi.org/10.1016/j.cej.2009.09.013.
[33] H. Freundlich, Over the adsorption in solution, J. Phys. Chem. *57* (385471) (1906) 1100–1107.
[34] E. Galiwango, H. A.Gabbar, Synergistic interactions, kinetic and thermodynamic analysis of co-pyrolysis of municipal paper and polypropylene waste, Waste Manag. *146* (2022) 86–93, https://doi.org/10.1016/j.wasman.2022.04.032.
[35] S. Ghanbari, A.M. Diaz, J. Park, H. Kang, C.H. Niu, Equilibrium and heat of water vapor adsorption on the surface of natural lignocellulose materials, Chem. Eng. Res. Des. *147* (2019) 18–29, https://doi.org/10.1016/j.cherd.2019.04.019.

[36] D. Guo, M. Hu, Z. Chen, B. Cui, Q. Zhang, Y. Liu, Y. Liu, Catalytic pyrolysis of rain tree biomass with nano nickel oxide synthetized from nickel plating slag: a green path for treating waste by waste, Bioresour. Technol. *315* (2020) 123831, https://doi.org/10.1016/j.biortech.2020.123831.
[37] H.B. Hadjltaief, M.B. Zina, M.E. Galvez, P. Da Costa, Photocatalytic degradation of methyl green dye in aqueous solution over natural clay-supported ZnO–TiO2 catalysts, J. Photochem. Photobiol. A: Chem. *315* (2016) 25–33.
[38] C. Hinz, Description of sorption data with isotherm equations, Geoderma *99* (3) (2001) 225–243, https://doi.org/10.1016/S0016-7061(00)00071-9.
[39] M. Hmoudah, A. El-Qanni, S. Abuhatab, N.N. Marei, A. El-Hamouz, B.J. A. Tarboush, M. Di Serio, Competitive adsorption of Alizarin Red S and Bromocresol Green from aqueous solutions using brookite TiO2 nanoparticles: experimental and molecular dynamics simulation, Environ. Sci. Pollut. Res. *29* (51) (2022) 77992–78008.
[40] W.-L. Hsu, S. Paul, J.A. Shamim, K. Kitaoka, H. Daiguji, Design and performance evaluation of a multilayer fixed-bed binder-free desiccant dehumidifier for hybrid air-conditioning systems: Part II – Theoretical analysis, Int. J. Heat. Mass Transf. *116* (2018) 1370–1378, https://doi.org/10.1016/j.ijheatmasstransfer.2017.09.080.
[41] V.J. Inglezakis, S.G. Poulopoulos, H. Kazemian, Insights into the S-shaped sorption isotherms and their dimensionless forms, Microporous Mesoporous Mater. *272* (2018) 166–176, https://doi.org/10.1016/j.micromeso.2018.06.026.
[42] M. Ismail, K. Akhtar, M. Khan, T. Kamal, M.A. Khan, A. M Asiri, S.B. Khan, Pollution, toxicity and carcinogenicity of organic dyes and their catalytic bio-remediation, Curr. Pharm. Des. *25* (34) (2019) 3645–3663.
[43] A. Jain, A. Ashma, K. Marazban, Expedient degradation of dye methyl green by enhanced photo–fenton process: a green chemical approach, J. Appl. Chem. *2* (2014) 13–25.
[44] E.A. Khan, Shahjahan, T.A. Khan, Synthesis of magnetic iron-manganese oxide coated graphene oxide and its application for adsorptive removal of basic dyes from aqueous solution: Isotherm, kinetics, and thermodynamic studies, Environ. Prog. Sustain. Energy *38* (s1) (2019) S214–S229, https://doi.org/10.1002/ep.12974.
[45] S. Khizar, M. Alomari, N. Zine, N. Jaffrezic-Renault, A. Errachid, A. Elaissari, Magnetic-responsive materials: properties, design, and applications, in: Stimuli-Responsive Materials for Biomedical Applications, Vol. 1436, American Chemical Society, 2023, pp. 53–79.
[46] R. Ladj, A. Bitar, M. Eissa, Y. Mugnier, R. Le Dantec, H. Fessi, A. Elaissari, Individual inorganic nanoparticles: preparation, functionalization and in vitro biomedical diagnostic applications, J. Mater. Chem. B *1* (10) (2013) 1381–1396, https://doi.org/10.1039/C2TB00301E.
[47] I. Langmuir, The adsorption of gases on plane surfaces of glass, mica and platinum, J. Am. Chem. Soc. *40* (9) (1918) 1361–1403, https://doi.org/10.1021/ja02242a004.
[48] E.C. Lima, A. Hosseini-Bandegharaei, J.C. Moreno-Piraján, I. Anastopoulos, A critical review of the estimation of the thermodynamic parameters on adsorption equilibria. Wrong use of equilibrium constant in the Van't Hoof equation for calculation of thermodynamic parameters of adsorption, J. Mol. Liq. *273* (2019) 425–434, https://doi.org/10.1016/j.molliq.2018.10.048.
[49] G. Limousin, J.P. Gaudet, L. Charlet, S. Szenknect, V. Barthès, M. Krimissa, Sorption isotherms: a review on physical bases, modeling and measurement, Appl. Geochem. *22* (2) (2007) 249–275, https://doi.org/10.1016/j.apgeochem.2006.09.010.
[50] X. Liu, S. An, X. Zhou, L. Zhang, Y. Zhang, W. Shi, J. Yang, Comparative studies of removal of methyl green and basic fuchsin from wastewater by a novel magnetic nanoparticles Mg-Ferrites, J. Dispers. Sci. Technol. *35* (12) (2014) 1727–1736, https://doi.org/10.1080/01932691.2013.871553.
[51] Y. M. Vargas-Rodríguez, A. Obaya, J. E. García-Petronilo, G. I. Vargas-Rodríguez, A. Gómez-Cortés, G. Tavizón, J. A. Chávez-Carvayar, Adsorption studies of aqueous solutions of methyl green for halloysite nanotubes: kinetics, isotherms, and thermodynamic parameters, Am. J. Nanomater. *9* (1) (2021) 1–11 (Retrieved from http://pubs.sciepub.com/).
[52] A.D. Manasrah, Ismail W. Almanassra, N.N. Marei, U.A. Al-Mubaiyedh, T. Laoui, M.A. Atieh, Surface modification of carbon nanotubes with copper oxide nanoparticles for heat transfer enhancement of nanofluids, RSC Adv. *8* (4) (2018) 1791–1802, https://doi.org/10.1039/C7RA10406E.
[53] A.D. Manasrah, T. Laoui, S.J. Zaidi, M.A. Atieh, Effect of PEG functionalized carbon nanotubes on the enhancement of thermal and physical properties of nanofluids, Exp. Therm. Fluid Sci. *84* (2017) 231–241, https://doi.org/10.1016/j.expthermflusci.2017.02.018.
[54] A.D. Manasrah, T. Montoya, A. Hassan, N.N. Nassar, Nanoparticles as Adsorbents for Asphaltenes, in: N.N. Nassar, F.B. Cortés, C.A. Franco (Eds.), Nanoparticles: An Emerging Technology for Oil Production and Processing Applications, Springer International Publishing, Cham, 2021, pp. 97–129.
[55] Marzougui, Z., Damak, M., Chaari, L., Ghrab, S., Elaissari, A., & Elleuch, B. (2021, 2021//). *Iron Removal from Groundwater by Adsorption Process onto Activated Carbon Obtained from Pinus halepensis Cone Wastes.* Paper presented at the Recent Advances in Environmental Science from the Euro-Mediterranean and Surrounding Regions (2nd Edition), Cham.
[56] A. Meghea, H.H. Rehner, I. Peleanu, R. Mihalache, Test-fitting on adsorption isotherms of organic pollutants from waste waters on activated carbon, J. Radioanal. Nucl. Chem. *229* (1) (1998) 105–110, https://doi.org/10.1007/BF02389456.
[57] S. Nizamuddin, M. Siddiqui, N. Mubarak, H.A. Baloch, E. Abdullah, S.A. Mazari, A. Tanksale, Iron oxide nanomaterials for the removal of heavy metals and dyes from wastewater, Nanoscale Mater. Water Purif. (2019) 447–472.
[58] S. Nizamuddin, M.T.H. Siddiqui, N.M. Mubarak, H.A. Baloch, E.C. Abdullah, S. A. Mazari, A. Tanksale, Chapter 17 - Iron oxide nanomaterials for the removal of heavy metals and dyes from wastewater, in: S. Thomas, D. Pasquini, S.-Y. Leu, D. A. Gopakumar (Eds.), Nanoscale Materials in Water Purification, Elsevier, 2019, pp. 447–472.
[59] N. Ouasfi, M. Zbair, S. Bouzikri, Z. Anfar, M. Bensitel, H. Ait Ahsaine, L. Khamliche, Selected pharmaceuticals removal using algae derived porous carbon: experimental, modeling and DFT theoretical insights, RSC Adv. *9* (17) (2019) 9792–9808, https://doi.org/10.1039/C9RA01086F.
[60] A. Panagopoulos, V. Giannika, Comparative techno-economic and environmental analysis of minimal liquid discharge (MLD) and zero liquid discharge (ZLD) desalination systems for seawater brine treatment and valorization, Sustain. Energy Technol. Assess. *53* (2022) 102477, https://doi.org/10.1016/j.seta.2022.102477.
[61] P. Panneerselvam, N. Morad, K.A. Tan, Magnetic nanoparticle (Fe3O4) impregnated onto tea waste for the removal of nickel (II) from aqueous solution, J. Hazard. Mater. *186* (1) (2011) 160–168.
[62] C.W. Park, E. Jeong, H.-M. Yang, H.-J. Kim, Helical magnetic micromotors decorated with nickel ferrocyanide for the active and rapid adsorption of radiocesium in water, Chemosphere *346* (2024) 140668, https://doi.org/10.1016/j.chemosphere.2023.140668.
[63] F. Parsaee, N. Fayzullaev, M.F. Nassar, B.A. Alreda, H.M.A. Mahmoud, A.G. Taki, M. Faraji, Co-Fe dual-atom isolated in N-doped graphydine as an efficient sulfur conversion catalyst in Li-S batteries, J. Alloy. Compd. *988* (2024) 174136, https://doi.org/10.1016/j.jallcom.2024.174136.
[64] N. Pichel, M. Vivar, M. Fuentes, The problem of drinking water access: a review of disinfection technologies with an emphasis on solar treatment methods, Chemosphere *218* (2019) 1014–1030, https://doi.org/10.1016/j.chemosphere.2018.11.205.
[65] M. Procházková, M. Touš, D. Horňák, V. Miklas, M. Vondra, V. Máša, Industrial wastewater in the context of European Union water reuse legislation and goals, J. Clean. Prod. *426* (2023) 139037, https://doi.org/10.1016/j.jclepro.2023.139037.
[66] N.U. Rahman, W. Bahadar, S. Alam, M. Zahoor, I. Zekker, F.A. Khan, H.C. A. Murthy, Activated sawdust-based adsorbent for the removal of basic blue 3 and methylene green from aqueous media, Adsorpt. Sci. Technol. *2022* (2022) 4551212, https://doi.org/10.1155/2022/4551212.
[67] X. Ren, C.-C. Wang, Y. Li, C.-Y. Wang, P. Wang, S. Gao, Ag(I) removal and recovery from wastewater adopting NH2-MIL-125 as efficient adsorbent: a 3Rs (reduce, recycle and reuse) approach and practice, Chem. Eng. J. *442* (2022) 136306, https://doi.org/10.1016/j.cej.2022.136306.
[68] K.S.M. Salih, P. Mamone, G. Dörr, T.O. Bauer, A. Brodyanski, C. Wagner, W. R. Thiel, Facile synthesis of monodisperse maghemite and ferrite nanocrystals from metal powder and octanoic acid, Chem. Mater. *25* (8) (2013) 1430–1435, https://doi.org/10.1021/cm303344z.
[69] K.S.M. Salih, W.R. Thiel, Palladium-catalyzed coupling reactions with magnetically separable nanocatalysts, Palladium-Catalyzed Coupling React. (2013) 57–78.
[70] E. Sharifpour, E. Alipanahpour Dil, A. Asfaram, M. Ghaedi, A. Goudarzi, Optimizing adsorptive removal of malachite green and methyl orange dyes from simulated wastewater by Mn-doped CuO-Nanoparticles loaded on activated carbon using CCD-RSM: Mechanism, regeneration, isotherm, kinetic, and thermodynamic studies, Appl. Organomet. Chem. *33* (3) (2019) e4768.
[71] R. Sips, Combined form of langmuir and Freundlich equations, J. Chem. Phys. *16* (429) (1948) 490–495.
[72] M. Smol, C. Adam, M. Preisner, Circular economy model framework in the European water and wastewater sector, J. Mater. Cycles Waste Manag. *22* (3) (2020) 682–697, https://doi.org/10.1007/s10163-019-00960-z.
[73] H. Suman, V.K. Sangal, M. Vashishtha, Treatment of tannery industry effluent by electrochemical methods: a review, Mater. Today.: Proc. *47* (2021) 1438–1444.
[74] A. Suwattanamala, N. Bandis, K. Tedsree, C. Issro, Synthesis, characterization and adsorption properties of Fe3O4 /MWCNT magnetic nanocomposites, Mater. Today.: Proc. *4* (5, Part 2) (2017) 6567–6575, https://doi.org/10.1016/j.matpr.2017.06.169.
[75] Y. Tian, B. Gao, V.L. Morales, H. Chen, Y. Wang, H. Li, Removal of sulfamethoxazole and sulfapyridine by carbon nanotubes in fixed-bed columns, Chemosphere *90* (10) (2013) 2597–2605, https://doi.org/10.1016/j.chemosphere.2012.11.010.
[76] M. Wahab, Z. Muhammad, S. Salman, A novel approach to remove ofloxacin antibiotic from industrial effluent using magnetic carbon nanocomposite prepared from sawdust of Dalbergia sissoo by batch and membrane hybrid technology, Membr. Technol. *27* (2019) 28.
[77] J. Wang, H. Chen, Catalytic ozonation for water and wastewater treatment: Recent advances and perspective, Sci. Total Environ. *704* (2020) 135249.
[78] J. Wang, X. Guo, Adsorption kinetic models: Physical meanings, applications, and solving methods, J. Hazard. Mater. *390* (2020) 122156, https://doi.org/10.1016/j.jhazmat.2020.122156.
[79] E. Worch, Adsorption Technology In Water Treatment: Fundamentals, Processes, and Modeling, Walter de Gruyter, 2012.
[80] N. Zatar, A. Abu Zuhri, N. Tayem, Quantitative determination of three textile reactive dyes in ground water, sewage water and soil using voltammetric and HPLC techniques, -Najah Univ. J. Res. - A (Nat. Sci.) *18* (2) (2004) 173–192, https://doi.org/10.35552/anujr.a.18.2.620.
[81] C. Zhao, J. Zhou, Y. Yan, L. Yang, G. Xing, H. Li, H. Zheng, Application of coagulation/flocculation in oily wastewater treatment: a review, Sci. Total Environ. *765* (2021) 142795, https://doi.org/10.1016/j.scitotenv.2020.142795.

[82] N.S. Riyaz, I. Badran, The catalytic thermo-oxidative decomposition of glimepiride using the isoconversional method, J Therm Anal Calorim 147 (2022) 10755–10765, https://doi.org/10.1007/s10973-022-11304-9.
[83] A. Zyoud, A.H. Zyoud, S.H. Zyoud, et al., Photocatalytic degradation of aqueous methylene blue using ca-alginate supported ZnO nanoparticles: point of zero charge role in adsorption and photodegradation, Environ Sci Pollut Res 30 (2023) 68435–68449, https://doi.org/10.1007/s11356-023-27318-1.
[84] H. Nassar, A. Zyoud, A. El-Hamouz, R. Tanbour, N. Halayqa, H.S. Hilal, Aqueous nitrate ion adsorption/desorption by olive solid waste-based carbon activated using ZnCl2, Sustainable Chemistry and Pharmacy 18 (2020) 100335.
[85] A.H. Zyoud, S.H. Zyoud, A. Amireh, An innovative and sustainable approach for water purification: Thermal decomposition of tetracycline contaminant adsorbed on thermally stable montmorillonite, Case Studies in Chemical and Environmental Engineering 9 (2024) 100631.
[86] H. Babas, G. Kaichouh, M. Khachani, M.E. Karbane, A. Chakir, A. Guenbour, A. Zarrouk, Equilibrium and kinetic studies for removal of antiviral sofosbuvir from aqueous solution by adsorption on expanded perlite: experimental, modelling and optimization, Surf Interfaces 23 (2021) 100962. Chicago.
[87] S. Ajebli, G. Kaichouh, M. Khachani, H. Babas, M. El Karbane, I. Warad, A. Zarrouk, The adsorption of Tenofovir in aqueous solution on activated carbon produced from maize cobs: Insights from experimental, molecular dynamics simulation, and DFT calculations, Chemical Physics Letters 801 (2022) 139676.
[88] S. Jodeh, R. Odeh, M. Sawalha, A.A. Obeid, R. Salghi, B. Hammouti, I. Warad, Adsorption of lead and zinc from used lubricant oil using agricultural soil: equilibrium, kinetic and thermodynamic studies, J. Mater. Environ. Sci 6 (2) (2015) 580–591.